

See discussions, stats, and author profiles for this publication at: <https://www.researchgate.net/publication/221871467>

Characterization of the Temporary Anion States on Perfluoroalkanes via Stabilized Koopmans' Theorem in Long-Range Corrected Density Functional Theory

ARTICLE *in* THE JOURNAL OF PHYSICAL CHEMISTRY A · FEBRUARY 2012

Impact Factor: 2.69 · DOI: 10.1021/jp211634w · Source: PubMed

CITATIONS

7

READS

54

3 AUTHORS, INCLUDING:



Ki Wi Chen

Tunghai University

12 PUBLICATIONS 115 CITATIONS

SEE PROFILE

Characterization of the Temporary Anion States on Perfluoroalkanes via Stabilized Koopmans' Theorem in Long-Range Corrected Density Functional Theory

Hsiu-Yao Cheng,* Chi-Wei Chen, and Chia-Hau Huang

Department of Chemistry, Tunghai University, Taichung 40704, Taiwan

ABSTRACT: The stabilized Koopmans' theorem (SKT) in long-range corrected density functional theory is used to characterize the temporary anion states of perfluoro-*n*-alkanes (*n*-PFAs) from C₂ to C₅, and perfluorocycloalkanes (*c*-PFAs) from C₃ to C₄. In this approach, stabilization is accomplished by varying the exponents of appropriate diffuse functions. The energies of temporary anion states are then identified by investigating the relationship between the resultant eigenvalues and scale parameter. The characteristics of resonance orbitals are also examined. For the lowest unfilled orbitals of perfluoroalkanes, results indicate that they are mainly from the π -bonding interactions between all neighboring C atoms. In addition, their energies decrease as the sizes of the perfluoroalkanes increase. Moreover, the energies of the *c*-C₃F₆/*c*-C₄F₈ are lower than those of the corresponding *n*-C₃F₈/*n*-C₄F₁₀. When compared with experimental data, our SKT calculations can yield conformable results. Thus, this SKT approach can provide more information on the resonance states of perfluoroalkanes.



1. INTRODUCTION

Perfluoroalkanes (PFAs) have aroused much scientific interest due to their wide applications. So far, they have been used as surfactants, dielectric fluids, cosolvents in supercritical extraction, industrial applications of plasma etching, and reaction media in green chemistry. PFAs have also been widely used in materials, biotechnology, organic synthesis, and fluorous biphasic chemistry.¹ Nevertheless, it is well-known that fluorine has a relatively small atomic radius and high electronegativity. The short, very strong, and highly polarized carbon–fluorine bond leads to some unusual properties of PFAs. For instance, these compounds are very stable and have long atmospheric lifetime. It is also true that the inertness and high infrared absorption properties make some PFAs the potent greenhouse gases. Since the reactions of C–F bond of PFAs rely on the transfer of electrons, the determination of electron attachment energies (AEs) is essential in studying the bonding, reactivity, and chemical properties of PFAs. In general, the vertical AEs can be determined by means of electron transmission spectroscopy (ETS) technique directly.^{2,3} Ishii et al. have carried out ETS measurements for PFAs, and they have indicated that the AEs of PFAs are generally positive (Table 7 in ref 4). Previous works of dissociative electron attachment, scattering cross-section, and theoretical studies have also reported that PFAs bind low-energy electrons.^{4–10}

Theoretical calculation of positive AEs is a challenging problem due to the fact that the anion is unstable with respect to electron detachment. The temporary anion state lies energetically above the ground state of the neutral molecule. Many computational methods have been developed for the studies of temporary anion states.^{3,11} In the Koopmans' theorem (KT) approximation, the AEs can be associated with the energies of the unfilled orbitals.¹² However, the energy

calculations of temporary anion states using the KT approximation are unreliable. Small basis sets in KT calculations cannot even account qualitatively for the relative energies of temporary anion states due to the artificial binding of the electron by the compact basis set. The KT approximation neither can generate definitive energies of temporary anion states by adopting a basis set with more diffuse functions. This is because the unfilled orbitals are prone to collapse onto approximations of continuum functions called orthogonalized discretized continuum (ODC)^{13–17} solutions.

To distinguish the temporary anion orbital solutions from the ODC solutions, the stabilization method proposed by Taylor and co-workers¹⁸ have been proposed. Their stabilization approach has been proved to yield accurate resonance energies for the model potential problems even with relatively small basis sets.¹⁹ In the stabilized Koopmans' theorem (SKT) approach introduced by Jordan and co-workers, the stabilization method is used in conjunction with Koopmans' theorem within the HF theory.^{13–16} This approach is generally very successful in predicting the relative AEs of isolated molecules when using flexible basis sets. In density functional theory (DFT),²⁰ most DFT potentials will not yield asymptotic behavior properly.^{11a,21} The errors for Koopmans' AEs in conventional DFT can be of several electron volts. Thus, various asymptotic correction schemes have been devised. In the long-range corrected (LRC) scheme, the coulomb operator is usually divided into short-range (SR) and long-range (LR) parts by using the standard error function.^{22–25} On the basis of the consideration of the integer discontinuity in the exact

Received: December 3, 2011

Revised: February 25, 2012

Published: February 29, 2012

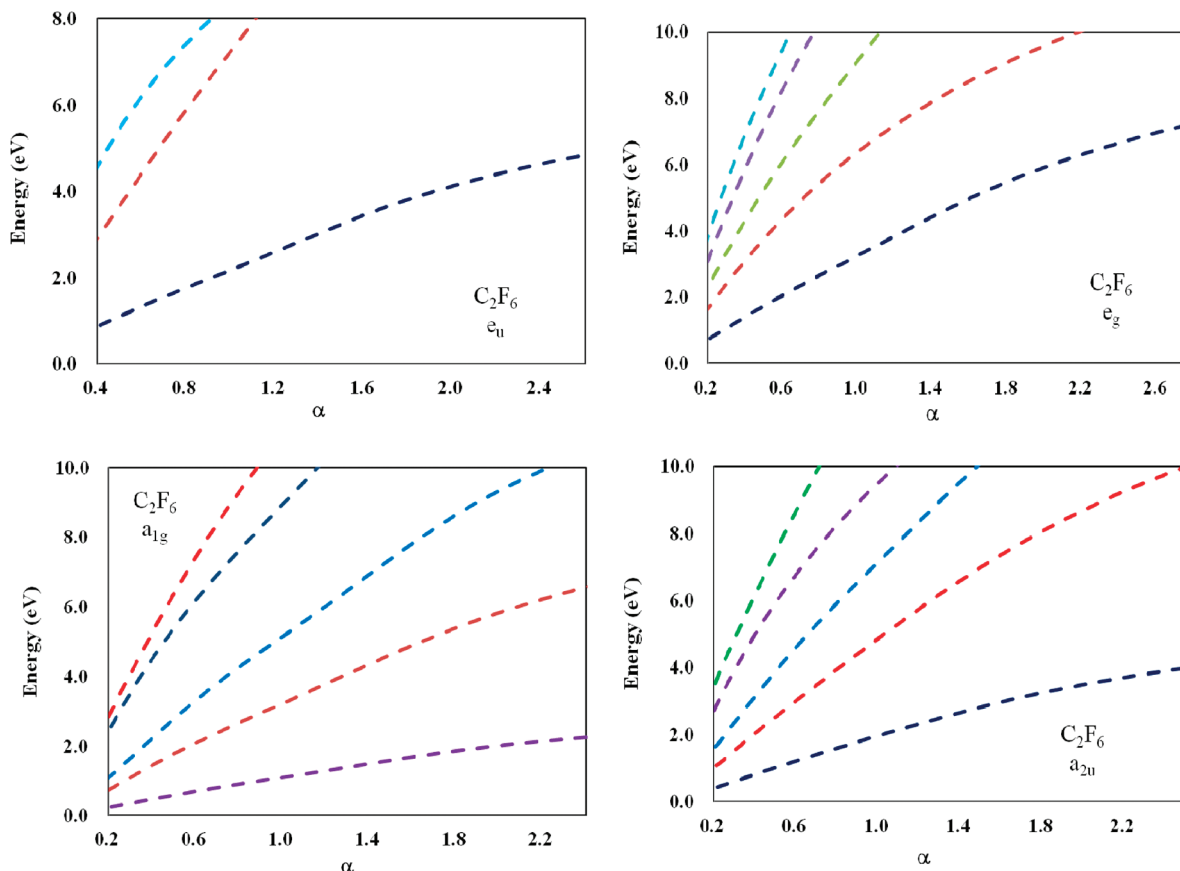


Figure 1. Energies of e_u , e_g , a_{1g} , and a_{2u} virtual orbitals of C_2F_6 as a function of α for a free electron in the absence of potentials using basis set A1.

exchange-correlation potential, Tozer and co-workers have proposed an alternative Koopmans-based approximation using asymptotic correction.²⁶ Recently, we have applied the stabilization method via DFT with asymptotically corrected potential in studying the temporary anion states of several molecules.²⁷ Results have indicated that our approach can yield improvements in predicting energies of temporary anion states over other approaches. Notice that the KT analogue approach for DFT is successful in predicting not only for the LUMO energies, but also for higher unfilled orbitals. One of the possible reasons is perhaps that the error of relative energies of unfilled orbitals maybe relatively unimportant when compared with experimental error.

So far, the temporary anion states of PFA molecules have been assigned by Ishii et al. using the KT HF/STO-3G calculation.⁴ However, the minimal basis set of the HF approach neglects relaxation and correlation effects. Hence, it may not be able to reliably predict the energies of the temporary anion states. Falcetta et al. used the stabilization method to characterize the temporary anion states of C_2F_6 .¹⁵ Yet, the stability of the temporary anion states for larger PFAs has not been established. Moreover, theoretical investigation for the unfilled orbitals of PFAs has been scarce. Hence, it is imperative to investigate the PFAs via the SKT method. In this article, the SKT calculations using LRC-DFT will be adopted to determine the energies of the unfilled orbitals that correspond to the temporary anion states of $n\text{-C}_n\text{F}_{2n+2}$ ($n = 2-5$), $c\text{-C}_3\text{F}_6$, and $c\text{-C}_4\text{F}_8$. The obtained results will also be compared with experimental values. It is hoped that the SKT approach can provide more information on the resonance states of PFAs.

2. COMPUTATIONAL METHOD

The vertical AE in the KT approximation can be written as $\text{AE}^{\text{KT}} \approx \varepsilon_{\text{VMO}}$, where ε_{VMO} denotes the virtual molecular orbital energy. The virtual orbital energy associated with the temporary anion state is also known as AE. The AE obtained from the KT approach will be denoted as ε_{VMO} . To distinguish the temporary anion state solutions from the virtual ODC ones, the stabilization method is employed.

In the application of the SKT method for the C_2F_6 calculations, eight different Gaussian-type basis sets, designated as A1, A2, A3, A4, A5, A6, B1, and B2 are employed. Our convention is denoted as follows. The basis set A1 denotes the 6-311+G(d) basis set with scaling of the exponents of diffuse + functions on the C and F atoms. The basis set A2 denotes the 6-311+G(d) with scaling of the exponents of the two outermost diffuse sp functions on the C and F atoms simultaneously. The basis set A3 is the 6-311+G(2d) with scaling of the exponents of diffuse + functions on the C and F atoms. The basis set A4 is the 6-311+G(2df) with scaling of the exponents of diffuse + functions on the C and F atoms. The basis set A5 is the 6-311+G(3d) with scaling of the exponents of diffuse + functions on the C and F atoms. The basis set A6 is the 6-311+G(3df) with scaling of the exponents of diffuse + functions on the C and F atoms. The basis set B1 is the aug-cc-pvdz basis set²⁸ with scaling of the outermost diffuse s and p functions on the C and F atoms. Finally, the basis set B2 denotes the aug-cc-pvtz basis set²⁸ with scaling of the outermost diffuse s and p functions on the C and F atoms.

The stabilization graphs are obtained by plotting the calculated energies (ε_{VMO}) as a function of the scale factor α .

With sufficiently flexible basis sets, one or more ODC solutions may approach the temporary anion orbital solutions in energy and can lead to avoided crossings between the two types of solutions as α increases. The unfilled orbitals corresponding to the temporary anion states are referred to as SKT levels.^{14,15} The energies of SKT levels can be extracted from the avoided crossings between the eigenvalues of the stabilization graph. In this study, the simplest midpoint method in Burrow et al. will be adopted.¹⁶ The energy of the SKT level is taken as the mean value of two eigenvalues involved in the avoided crossing at the α_{ac} of the closest approach.²⁹ If the SKT level is well separated from ODC ones over the range of alpha values, the energy of the resonance state can also be estimated simply from the inspection of stabilization graphs.¹⁵

For LRC functional, we use LC- ω PBE, ω B97XD, CAM-B3LYP, LC-PBEPBE, LC-TPSSTPSS, LC-BLYP, LC-B97D, and LC-M06L functionals. The LC- ω PBE²² functional contains SR ω PBE exchange, LR HF exchange, and full range PBE correlation. The ω B97XD²³ functional includes LR HF exchange, a small fraction of SR HF exchange, a modified B97 SR exchange, B97 correlation density functional, and empirical dispersion corrections. The CAM-B3LYP²⁴ functional comprises 0.19 HF plus 0.81 Becke 1988 (B88) exchange interaction at SR and 0.65 HF plus 0.35 B88 at LR. The LC-PBEPBE, LC-TPSSTPSS, LC-BLYP, LC-B97D, and LC-M06L are obtained by applying the LR correction of Hiraoka and co-workers²⁵ to the pure PBEPBE,³⁰ TPSSTPSS,³¹ BLYP, B97D, and M06L³² functionals. In addition, the double-hybrid functionals B2PLYP-D³³ that contain second-order perturbation corrections with LR dispersion terms will also be employed.

All calculations are performed using the Gaussian09 program.³⁴ Geometric optimizations of all molecules are carried out at the B3LYP/6-311+G(d) level. The geometries of C_2F_6 , C_3F_8 , n - C_4F_{10} , n - C_5F_{12} , c - C_3F_6 , and c - C_4F_8 are optimized under D_{3d} , C_{2v} , C_{2h} , C_{2v} , D_{3h} , and D_{2d} symmetry constraints. The symmetry in the labeling of the orbital is based on the z axis being along the principal axis. The optimized geometries are confirmed to be of real minima via frequency analysis. However, in each case of n - C_4F_{10} and n - C_5F_{12} , the C_{2h} or C_{2v} geometric optimization always converges with one imaginary frequency. The frequency is associated with the internal rotation of the $-CF_3$ group. Although the C_{2h} or C_{2v} geometry is not of global minimum, its calculated orbital energies differ only slightly (<0.1 eV) from that of the C_1 geometry of global minimum. For the C–C bonds of linear-chain PFAs, the optimized bond lengths are 1.557, 1.561, and 1.568 Å for C_2F_6 , C_3F_8 , and n - C_5F_{12} , respectively. The optimized bond lengths for the central C–C bond and outer C–C bonds are 1.566 and 1.564 Å for n - C_4F_{10} , respectively. As for the C–F bonds, the optimized bond lengths for $-CF_2$ units and $-CF_3$ groups are 1.349–1.352 and 1.335–1.337 Å for all PFAs, respectively. As for c -PFAs, the optimized C–C and C–F bond lengths are 1.527 and 1.336 Å for c - C_3F_6 and 1.577 and 1.337 Å for c - C_4F_8 , respectively.

3. RESULTS AND DISCUSSION

First, we will present the results of C_2F_6 molecule. In the D_{3d} point group, the C_2F_6 molecule has six a_{1g} , six a_{2u} , five-pair e_g , and five-pair e_u occupied orbitals. The SKT calculations are performed for the LC- ω PBE, ω B97XD, CAM-B3LYP, LC-PBEPBE, LC-TPSSTPSS, LC-BLYP, LC-B97D, LC-M06L, and B2PLYP-D methods using basis set A1 on the unfilled orbitals.

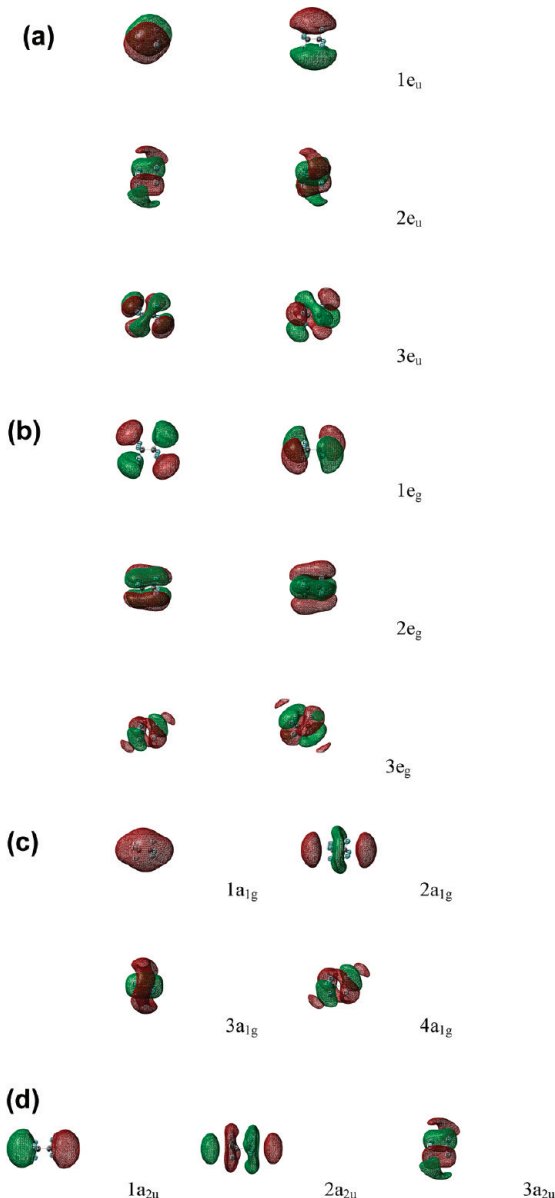


Figure 2. Plots of the first (a) three e_u , (b) three e_g , (c) four a_{1g} , and (d) three a_{2u} virtual orbitals of C_2F_6 for a free electron in the absence of potentials at $\alpha = 1.0$. The isosurface values are chosen to be 0.02 for all the orbital plots.

In order to distinguish the resonance from the ODC solutions of the molecular system, the so-called one-electron discretized continuum (1e-DC)¹⁵ solutions for a free electron are invoked. The energies of the 1e-DC solutions are obtained by solving the one-electron Schrödinger equation as described by the molecular basis set in the absence of any potential.^{14b,15} Figure 1 shows the energies of the 1e-DC solutions as a function of scale factor α for the e_u , e_g , a_{1g} , and a_{2u} virtual orbitals of C_2F_6 located at the appropriate nuclear position using basis set A1. As shown in Figure 1, all 1e-DC solutions increase with α . We then examine the characteristics of 1e-DC solutions. Figure 2a–d illustrates the first three e_u , three e_g , four a_{1g} , and three a_{2u} 1e-DC solutions at $\alpha = 1.0$, respectively. The comparison of the energies and characteristics of the 1e-DC solutions with those of the virtual orbitals from DFT calculations of molecules can let us determine the possible temporary anion states.¹⁵

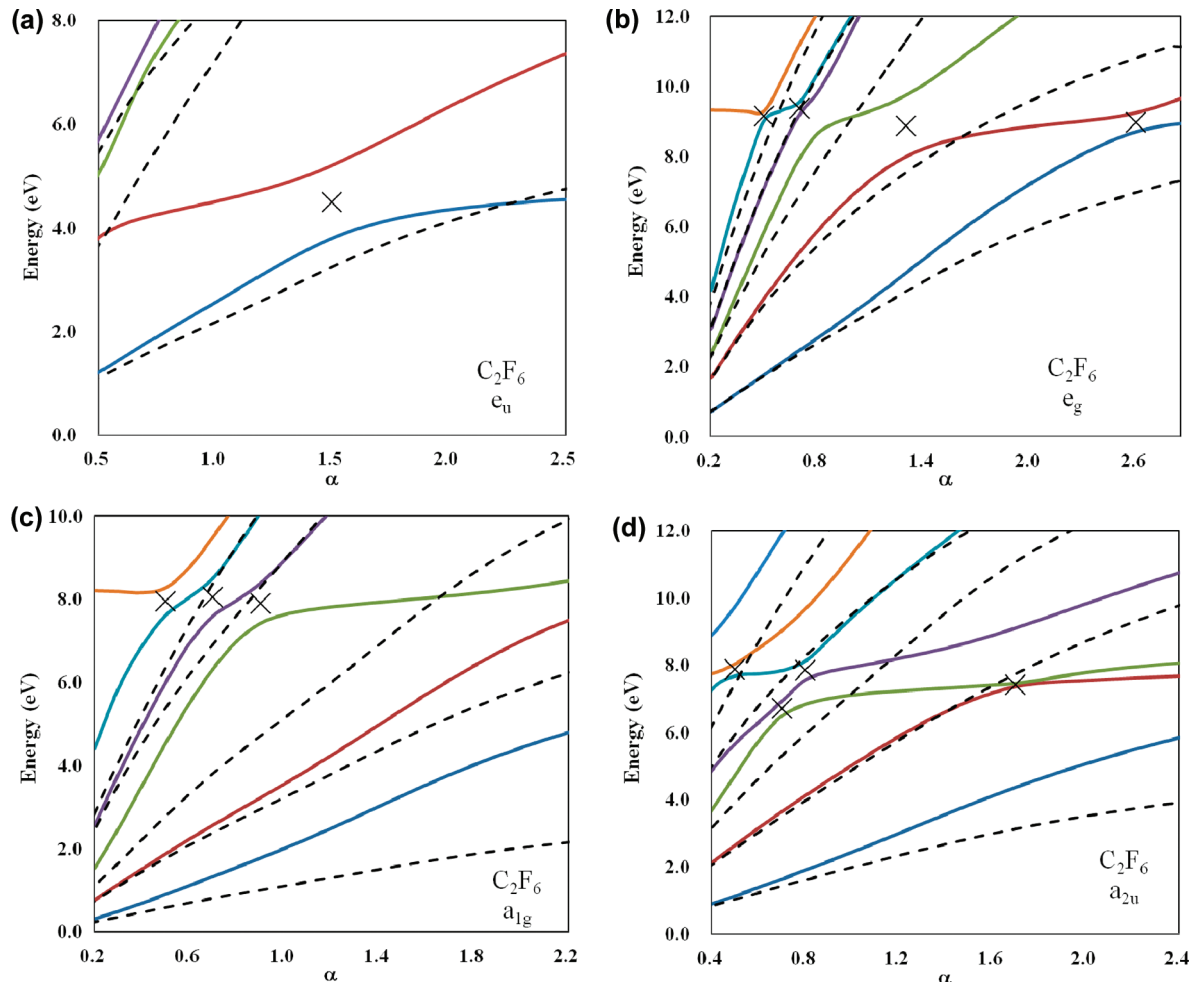


Figure 3. Stabilization graphs for C_2F_6 via SKT^{LC- ω PBE} method using basis set A1. Energies of (a) e_u (b) e_g (c) a_{1g} and (d) a_{2u} virtual orbitals (represented by the solid curves) and the free electron (represented by the dashed curves) as a function of α . The locations of α_{ac} are marked with X.

The stabilization graphs for the e_u , e_g , a_{1g} and a_{2u} virtual orbitals of C_2F_6 and the 1e-DC solutions calculated via the SKT LC- ω PBE (denoted as SKT^{LC- ω PBE}) method using basis set A1 are shown in Figure 3a–d. There are two types of energies for virtual orbital solutions in the stabilization calculations. One is the unfilled orbital solution and the other the ODC virtual orbital solution. They are readily distinguished by examining how their energies are varied with α and by comparing their solutions with the 1e-DC solutions. As shown in Figure 3a–d, the energies of ODC generally lie above those of the 1e-DC when the SKT^{LC- ω PBE} method is used. Previous SKT-HF and S- Δ MP2 studies by Jordan et al. have also obtained the same results.¹⁵ We will start with the results of the e_u virtual orbitals. In Figure 3a, the first solution for $\alpha > 1.5$ and second solution for $\alpha < 1.5$ that remain almost constant are mainly from the $6e_u$ orbital solution. The first solution for $\alpha < 1.5$ and second solution for $\alpha > 1.5$ are mainly from the first e_u ODC solution, the third solution is mainly from the second e_u ODC solution, and the fourth one is mainly from the third e_u ODC solution. The avoided crossing resulted from the coupling between the first and second solutions is located at $\alpha_{ac}(1,2) = 1.5$. The energy of the $6e_u$ obtained from the avoided crossing is 4.50 eV at $\alpha_{ac}(1,2)$. Figure 4a displays the first four e_u virtual orbitals of C_2F_6 for $\alpha = 1.0$. On the basis of the analysis of the nature of virtual orbitals, the second e_u virtual orbitals are mainly from the $6e_u$ orbitals. As can be seen in Figure 4a, the $6e_u$ orbitals are

essentially from C–C π and C–F σ^* . While the first, third, and fourth e_u virtual orbitals are mainly from their first three ODC solutions. The diffuse characteristics of the first three ODC solutions are similar to those of the first three 1e-DC solutions as shown in Figures 2a and 4a.

In Figure 3b, the second solution for $1.3 < \alpha < 2.6$, third solution for $0.9 < \alpha < 1.3$, fifth solution for $0.5 < \alpha < 0.7$, and sixth solution for $\alpha < 0.5$ are mainly from the $6e_g$ orbital solution. Four avoided crossings are found in Figure 3b. They are from the couplings between $6e_g$ orbitals and the first, second, fourth, and fifth ODC solutions. The locations of them are at $\alpha_{ac}(1,2) = 2.6$, $\alpha_{ac}(2,3) = 1.3$, $\alpha_{ac}(4,5) = 0.7$, and $\alpha_{ac}(5,6) = 0.5$, respectively. Their corresponding energies are 8.97 eV at $\alpha_{ac}(1,2)$, 8.87 eV at $\alpha_{ac}(2,3)$, 9.37 eV at $\alpha_{ac}(4,5)$, and 9.15 eV at $\alpha_{ac}(5,6)$, respectively. The average of each set of these energy values will be defined as the energy of the $6e_g$ orbitals. Thus, after taking the average, the energy of the $6e_g$ orbitals is 9.09 eV. Figure 4b displays the first four e_g virtual orbitals of C_2F_6 for $\alpha = 1.0$. In this figure, the third e_g virtual orbitals are mainly from the $6e_g$ orbitals, and they are largely C–C π^* in nature. However, the first, second, and fourth e_g virtual orbitals are mainly from their first three ODC solutions. They are similar to those of the first three 1e-DC solutions as shown in Figures 2b and 4b.

In Figure 3c, the first and second solutions are mainly from the first and second a_{1g} ODC solutions. The third solution for α

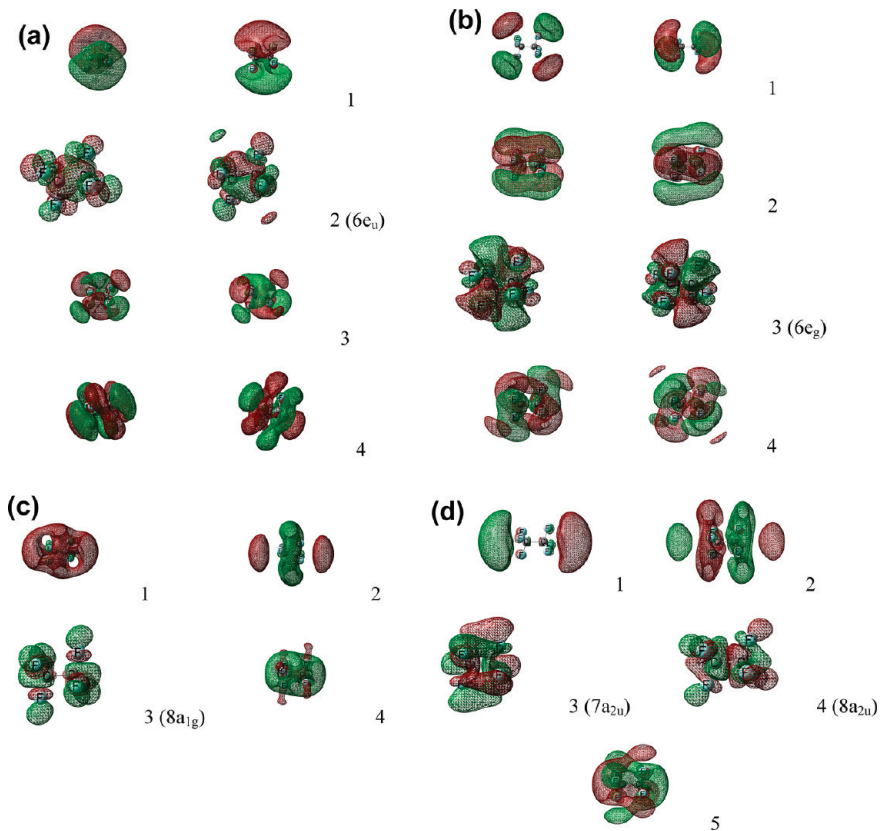


Figure 4. Plots of the first (a) four e_u , (b) four e_g , (c) four a_{1g} , and (d) five a_{2u} virtual orbitals at $\alpha = 1.0$ for C_2F_6 . The isosurface values are chosen to be 0.02 for all the MO plots.

> 0.9 and the sixth solution for $\alpha < 0.5$ that remain almost constant (~ 8.0 eV) are mainly from the $8a_{1g}$ orbital solution. The energies of the $8a_{1g}$ orbital obtained are 7.90, 8.05, and 7.95 eV at $\alpha_{ac}(3,4) = 0.9$, $\alpha_{ac}(4,5) = 0.7$, and $\alpha_{ac}(5,6) = 0.5$, respectively. Thus, the energy of the $8a_{1g}$ orbital is 7.97 eV. Figure 4c displays the first four a_{1g} orbitals of C_2F_6 for $\alpha = 1.0$. As indicated in this figure, the third a_{1g} virtual orbital is from the $8a_{1g}$ orbital, which is mainly derived from C–F σ^* with low amplitude between C atoms. The first, second, and fourth a_{1g} orbitals are from the first three ODC solutions, which are similar to those of the first three 1e-DC solutions as shown in Figures 2c and 4c.

In Figure 3d, the stabilization graph has two resonance solutions and five DC solutions. According to our observation, the third solution for $0.7 < \alpha < 1.7$ and fifth solution for $0.5 < \alpha < 0.8$ are mainly from the $7a_{2u}$ and $8a_{2u}$ orbital solutions, respectively. The first solution corresponds to the first ODC solution. The second solution for $\alpha < 1.7$ is mainly from the second ODC solution. The fifth solution for $\alpha > 0.8$ and sixth solution for $\alpha > 0.5$ are mainly from the third ODC and fourth ODC solutions, respectively. The seventh solution is mainly from the fifth ODC solution. The energies obtained for the $7a_{2u}$ orbital are 7.41 eV at $\alpha_{ac}(2,3) = 1.70$ and 6.71 eV at $\alpha_{ac}(3,4) = 0.7$. The energies obtained for the $8a_{2u}$ orbital are 7.84 eV at $\alpha_{ac}(4,5) = 0.8$ and 7.86 eV at $\alpha_{ac}(5,6) = 0.5$. Thus, the energies of the $7a_{2u}$ and $8a_{2u}$ orbitals are 7.06 and 7.85 eV, respectively. The resonance energies can also be estimated from the stabilized energy values. The stabilized energy values for $7a_{2u}$ and $8a_{2u}$ (~ 7.2 and 7.9 eV) are close to those obtained from the midpoint method. Figure 4d displays the first five a_{2u} virtual orbitals of C_2F_6 for $\alpha = 1.0$. As indicated in this figure, the third

and fourth a_{2u} virtual orbitals are mainly from the $7a_{2u}$ and $8a_{2u}$ orbitals. They are mainly derived from C–F σ^* and C–C σ^* . The first, second, and fifth a_{2u} virtual orbitals are mainly from the first, second, and third ODC solutions as shown in Figures 2d and 4d.

The results of AEs of C_2F_6 using various SKT and KT methods are tabulated along with the experimental values in Table 1. To compare with experimental results, corrected AEs are also included in the table. The corrected values are obtained by shifting the amount from the calculated AE values to bring the LUMOs of C_2F_6 into agreement with the experimental values of Ishii et al.⁴ As can be seen from the table, the AEs obtained via the SKT ω B97XD and CAM-B3LYP methods are smaller than those obtained from the other LRC-DFT methods. Possible reasons for these discrepancies are due to the different considerations of exchange-correlation potential, self-interaction effect, long-range dispersion corrections, and Coulomb contributions at large electron-molecule distance among various methods.³⁵ The AEs obtained from previous SKT HF method¹⁵ are larger than those obtained from all of the DFT methods for C_2F_6 . One possible reason for the overestimation of the HF method is its neglect of electron correlation effects. When the KT method is used, the lowest virtual orbitals of the symmetry of interest may not correspond to temporary anion states. Nevertheless, according to Table 1, the differences for AE values obtained from the temporary anion states in KT calculations with those obtained from the SKT method are within 0.7 eV for the LRC-DFT methods. As can be seen from Table 1 for the SKT LC- ω PBE, LC-PBEPBE, LC-TPSSTPSS, and LC-BLYP calculations, the AEs obtained are 4.5–4.6 eV for $6e_u$ orbitals, 7.1–8.0 eV for $7a_{2u}$ $8a_{2u}$, and

Table 1. Calculated and Corrected^a AEs (eV) for C₂F₆ Using Basis Set A1

	method	6e _u	7a _{2u}	8a _{2u}	8a _{1g}	6e _g
SKT	LC- ω PBE	4.50 (4.60)	7.06 7.16	7.85 7.95	7.97 8.07	9.09 9.19)
	ω B97XD	3.68 (4.60)	6.43 7.35	6.99 7.91	7.15 8.07	8.38 9.30)
	CAM-B3LYP	3.06 (4.60)	5.85 7.39	6.33 7.87	6.50 8.04	7.56 9.10)
	LC-PBEPBE	4.51 (4.60)	7.10 7.19	7.90 7.99	7.85 7.94	9.02 9.11)
	LC-TPSSTPSS	4.56 (4.60)	7.20 7.24	7.96 8.00	8.02 8.06	9.11 9.15)
	LC-BLYP	4.61 (4.60)	7.16 7.15	7.83 7.82	7.85 7.84	9.28 9.27)
	LC-B97D	4.12 (4.60)	6.83 7.31	7.45 7.93	7.67 8.15	8.79 9.27)
	LC-M06L	4.15 (4.60)	7.14 7.59	7.75 8.20	8.13 8.58	8.73 9.18)
	B2-PLYPD	3.93 (4.60)	6.84 7.51	7.05 7.72	7.22 7.89	8.58 9.25)
	SKT (HF) ^b	7.4	10.9	11.6	11.4	12.3
KT	S-DMP2 ^b	4.1	7.9	8.7	8.0	9.5
	exptl ^c	4.60	8.86 (with width ~3 eV)			
	exptl ^d	4.7	8.5			

^aThe corrected values (shown in parentheses) are obtained by shifting the amount needed to bring the calculated AEs into agreement with experimental values of ref 4 for the LUMOs. ^bReference 15.

^cReference 4. ^dReference 7.

8a_{1g} orbitals, and 9.0–9.3 eV for 6e_g orbitals. These predictions are in accord with previous studies.^{4,7,15} For instance, previous S-DMP2 studies by Jordan et al. identified the resonances at 4.1, 7.9, 8.0, 8.7, and 9.5 eV (Table 2 of ref 15). The ET spectrum studied by Ishii et al.⁴ displayed resonances at 4.6 and 8.9 eV, while the latter having a resonance width of about 3 eV. The scattering cross-section studied by Tossell et al.⁷ exhibited resonance enhancement at 4.7 and 8.5 eV. For the assignments of the shape resonance observed in ET spectrum on C₂F₆, the electron capture into 6e_u orbitals corresponds to the resonance at 4.6 eV in the ET spectrum. The very broad resonances at 8.86 eV can be associated with the electron capture into 7a_{2u}, 8a_{2u}, 8a_{1g}, and 6e_g orbitals. In summary, our SKT calculations can provide support for the assignments of features observed in the ET spectrum of C₂F₆ made by Jordan et al.¹⁵

Table 2 tabulates the calculated AEs of C₂F₆ using different basis sets for the representative SKT^{LC- ω PBE} method. The AEs vary by 0.0–0.2 eV for unfilled orbitals in all basis sets. Our

calculations have revealed that the 6-311+G(d) basis sets A1 and A2 are sufficiently flexible to characterize the anion states of C₂F₆. The inclusion of additional diffuse d or f polarization functions on C and F is of minor importance. These findings are in good agreement with those of the previous studies by Jordan et al.¹⁵ They have indicated that the basis set A2 is sufficiently flexible to describe the valence-like SKT levels of C₂F₆.

As for C₃F₈, n-C₄F₁₀, and n-C₅F₁₂, the SKT calculations are performed for the LC- ω PBE, LC-TPSSTPSS, and LC-BLYP methods using basis set A1. Simple molecular orbital considerations lead one to expect C₃F₈, n-C₄F₁₀, and n-C₅F₁₂ will have 10, 13, and 16 valence-type unfilled MOs, respectively. We will first present the results of the C₃F₈ molecule. It has 16 a₁, 7 a₂, 10 b₁, and 12 b₂ occupied orbitals in the C_{2v} point group. The stabilization graphs of C₃F₈ for the a₁, a₂, b₁, and b₂ virtual orbitals and the 1e-DC solutions via the SKT^{LC- ω PBE} method using basis set A1 are shown in Figure 5a–d. Ten unfilled orbitals (17a₁–20a₁, 8a₂, 11b₁–12b₁, and 13b₂–15b₂) are found to be below 10 eV. In Figure 5a, the stabilization graph has four a₁ resonance solutions. In this figure, the first solution for $\alpha > 1.5$, fifth solution for 0.7 < $\alpha < 0.9$, and sixth solution for $\alpha < 0.7$ are mainly from the 8a₁ orbital solution. The fourth solution for $\alpha > 2.7$, fifth solution for 2.2 < $\alpha < 2.7$, sixth solution for 1.8 < $\alpha < 2.2$, and seventh solution for 0.8 < $\alpha < 1.8$ are mainly from the 9a₁ orbital solution. The sixth solution for 2.2 < $\alpha < 2.8$ and eighth solution for 0.9 < $\alpha < 1.5$ are mainly from the 10a₁ orbital solution. The seventh solution for $\alpha > 2.2$, eighth solution for 1.5 < $\alpha < 2.2$, and ninth solution for 1.1 < $\alpha < 1.5$ are mainly from the 11a₁ orbital solution. For the energy range between 4.0 and 6.0 eV, the second to eighth solutions correspond to the first to seventh ODC solutions. The energies obtained for the 8a₁ orbital are 3.53 eV at $\alpha_{ac}(4,5) = 0.9$ and 3.24 eV at $\alpha_{ac}(5,6) = 0.7$. The energies obtained for the 9a₁ orbital are 8.00 eV at $\alpha_{ac}(4,5) = 2.7$, 7.77 eV at $\alpha_{ac}(5,6) = 2.2$, 7.72 eV at $\alpha_{ac}(6,7) = 1.8$, and 6.72 eV at $\alpha_{ac}(8,9) = 0.7$. The energies obtained for the 10a₁ orbital are 8.33 eV at $\alpha_{ac}(5,6) = 2.9$ and 7.47 eV at $\alpha_{ac}(8,9) = 0.9$. The energies obtained for the 11a₁ orbital are 8.90 eV at $\alpha_{ac}(6,7) = 3.1$, 8.77 eV at $\alpha_{ac}(7,8) = 2.2$, 8.64 eV at $\alpha_{ac}(8,9) = 1.5$, and 8.57 eV at $\alpha_{ac}(9,10) = 1.1$. Thus, the obtained energies of the 8a₁, 9a₁, 10a₁, and 11a₁ orbitals are 3.39, 7.55, 7.90, and 8.72 eV, respectively. In Figure 5a, the avoided crossing pattern is quite complex, and more than two states are interacting simultaneously. Hence, in order to compare with the obtained energies, the density of states (DOS) analysis introduced by Mandelshtam et al.^{29b} is also performed in these cases. Our DOS analysis procedure follows the one proposed in the appendix of ref 15. The obtained energies of the 8a₁, 9a₁, 10a₁, and 11a₁ orbitals from the DOS analysis are 3.36, 7.48, 7.86, and 8.74 eV, respectively. These values are very close to the aforementioned results. In Figure 5b, the first and second solutions for $\alpha > 1.8$ are mainly from the 8a₂ orbital solution

Table 2. Calculated AEs (eV) of C₂F₆ Using the SKT^{LC- ω PBE} Method

	basis set	A1	A2	A3	A4	A5	A6	B1	B2
C ₂ F ₆	6e _u	4.50	4.50	4.57	4.58	4.42	4.56	4.58	4.58
	7a _{2u}	7.06	7.04	7.11	7.22	7.16	7.20	7.07	7.14
	8a _{2u}	7.85	7.79	7.91	7.93	7.93	8.02	7.90	7.91
	8a _{1g}	7.97	7.93	8.02	8.18	8.04	8.20	8.02	8.08
	6e _g	9.09	9.00	9.17	9.19	9.13	9.24	9.24	9.21

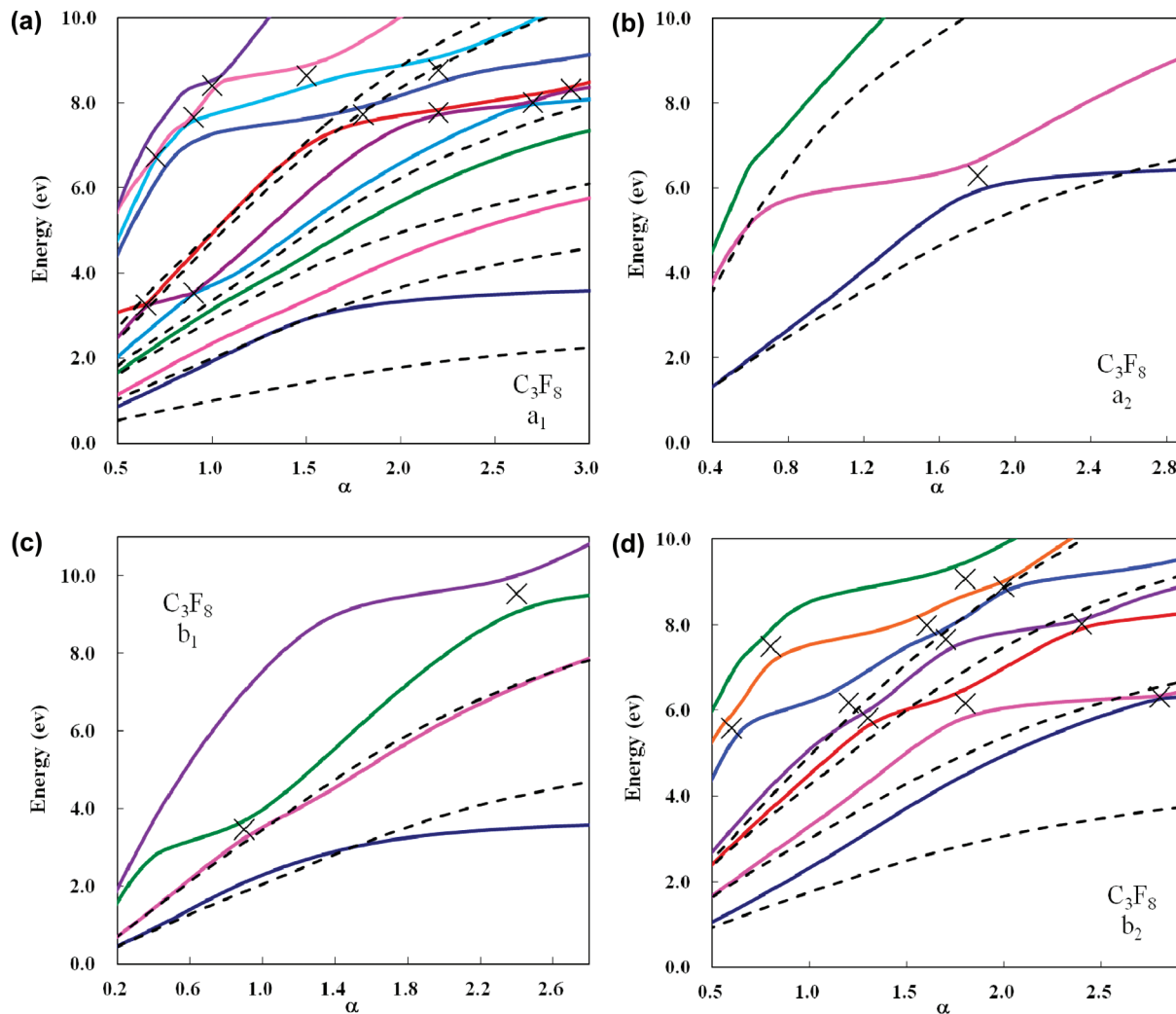


Figure 5. Stabilization graphs for C_3F_8 via the SKT^{LC- ω PBE} method using basis set A1. Energies of (a) a_1 , (b) a_2 , (c) b_1 , and (d) b_2 virtual orbitals (represented by the solid curves) and the free electron (represented by the dashed curves) as a function of α . The locations of α_{ac} are marked with \times .

and the first a_2 ODC solution, respectively. The energies of the $8a_2$ obtained from the avoided crossings are 6.28 eV at $\alpha_{ac}(1,2) = 1.8$. In Figure 5c, the first solution for $\alpha > 0.9$ and third solution for $\alpha > 2.4$ are mainly from the $11b_1$ and $12b_1$ solutions, respectively. The energy of the $11b_1$ obtained from the avoided crossing is 3.46 eV at $\alpha_{ac}(2,3) = 0.9$. The energy obtained for $12b_1$ orbital is 9.54 eV at $\alpha_{ac}(3,4) = 2.4$. In Figure 5d, the first solution for $\alpha > 2.8$, second solution for $1.8 < \alpha < 2.8$, third solution for $1.3 < \alpha < 1.8$, and fifth solution for $0.6 < \alpha < 1.2$ are mainly from the $13b_2$ orbital solution. The third solution for $\alpha > 2.4$, fourth solution for $1.7 < \alpha < 2.4$, and sixth one for $0.8 < \alpha < 1.6$ are mainly from the $14b_2$ orbital solution. The seventh solution for $1.0 < \alpha < 1.8$ and the fifth solution for $\alpha > 2.0$ are mainly from the $15b_2$ orbital solution. The energies of the $13b_2$ obtained from the avoided crossings are 6.31 eV at $\alpha_{ac}(1,2) = 2.8$, 6.16 eV at $\alpha_{ac}(2,3) = 1.8$, 5.82 eV at $\alpha_{ac}(3,4) = 1.3$, 6.19 eV at $\alpha_{ac}(4,5) = 1.2$, and 5.58 eV at $\alpha_{ac}(5,6) = 0.6$. The energies obtained for the $14b_2$ orbital are 8.01 eV at $\alpha_{ac}(3,4) = 2.4$, 7.65 eV at $\alpha_{ac}(4,5) = 1.7$, 7.99 eV at $\alpha_{ac}(5,6) = 1.6$, and 7.49 eV at $\alpha_{ac}(6,7) = 0.8$. The energies obtained for the $15b_2$ orbital are 8.89 eV at $\alpha_{ac}(5,6) = 2.0$ and 9.07 eV at $\alpha_{ac}(6,7) = 1.8$. Thus, the obtained energies of the $13b_2$, $14b_2$, and $15b_2$ orbitals are 6.01, 7.79, and 8.98 eV, respectively.

Figure 6 displays the $17a_1$, $19a_1$, $8a_2$, $11b_1$, $12b_1$, $13b_2$, $14b_2$, and $15b_2$ SKT orbitals for $\alpha = 2.0$ and $18a_1$ and $20a_1$ SKT orbitals for $\alpha = 1.0$ of C_3F_8 . As can be seen in Figure 6, the LUMO $17a_1$ is essentially from a π -bonding interaction between all neighboring C atoms. The $18a_1$ and $19a_1$ orbitals are essentially from σ^*_{CF} and σ^*_{CC} . The $20a_1$ orbital is mainly from σ^*_{CF} . The $8a_2$ orbital is essentially from σ^*_{CF} and π_{CC} . The $13b_2$ orbital is essentially from σ^*_{CF} mixing with C(p). The $14b_2$ orbital is mainly derived from two $-CF_3$ groups. The $15b_2$ orbital is essentially from σ^*_{CF} and π^*_{CF} . The $11b_1$ orbital is largely from π_{CC} . The $12b_1$ orbital is essentially from π^*_{CC} , π^*_{CF} , and σ^*_{CF} .

Next for the $n\text{-C}_4\text{F}_{10}$ molecule, it has $18 a_g$, $11 a_u$, $11 b_g$, and $17 b_u$ occupied orbitals in the C_{2h} point group. The stabilization graphs for the a_g , a_u , b_g , and b_u virtual orbitals of $n\text{-C}_4\text{F}_{10}$ via the SKT^{LC- ω PBE} method using basis set A1 are shown in Figure 7a–d. In Figure 7a, the energy obtained for the $19a_g$ orbital is 5.82 eV at $\alpha_{ac}(4,5) = 1.5$. The energies obtained for the $20a_g$ orbital are 7.95 eV at $\alpha_{ac}(4,5) = 2.5$, 7.90 eV at $\alpha_{ac}(5,6) = 2.1$, 7.68 eV at $\alpha_{ac}(7,8) = 1.4$, and 7.50 eV at $\alpha_{ac}(8,9) = 0.9$. The energies obtained for the $21a_g$ orbital are 8.45 eV at $\alpha_{ac}(10,11) = 1.0$ and 8.40 eV at $\alpha_{ac}(11,12) = 0.8$. The energies obtained for the $22a_g$ orbital are 8.68 eV at $\alpha_{ac}(7,8) = 2.0$, 8.65 eV at $\alpha_{ac}(8,9) = 1.6$, and 8.56 eV at $\alpha_{ac}(9,10) = 1.1$. Thus, the obtained energies of

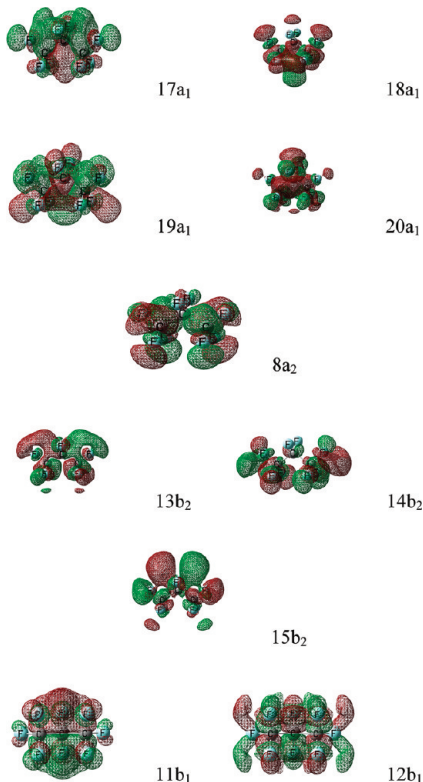


Figure 6. Plots of the $17a_1$, $19a_1$, $8a_2$, $13b_2$, $14b_2$, $15b_2$, $11b_1$, and $12b_1$ SKT orbitals at $\alpha = 2.0$ and the $18a_1$ and $20a_1$ SKT orbitals at $\alpha = 1.0$ for C_3F_8 . The isosurface values are chosen to be 0.02 for all the MO plots.

the $19a_g$, $20a_g$, $21a_g$, and $22a_g$ orbitals are 5.82, 7.76, 8.43, and 8.63 eV, respectively. In Figure 7b, the energy of the $12a_u$ obtained from the avoided crossing is 2.69 eV at $\alpha_{ac}(2,3) = 0.6$. The energies obtained for the $13a_u$ orbital are 7.52 eV at $\alpha_{ac}(2,3) = 2.6$ and 7.31 eV at $\alpha_{ac}(3,4) = 1.7$. Thus, the obtained energy of the $13a_u$ orbital is 7.42 eV. In Figure 7c, the energy of the $12b_g$ obtained from the avoided crossing is 4.93 eV at $\alpha_{ac}(2,3) = 1.3$. The energy of the $13b_g$ obtained from the avoided crossing is 10.02 eV at $\alpha_{ac}(3,4) = 2.6$. In Figure 7d, the energy of the $18b_u$ obtained from the avoided crossing is 2.49 eV at $\alpha_{ac}(5,6) = 0.5$. The $19b_u$ obtained from the avoided crossings are 6.70 eV at $\alpha_{ac}(3,4) = 2.5$, 6.41 eV at $\alpha_{ac}(5,6) = 1.6$, 6.60 eV at $\alpha_{ac}(7,8) = 1.0$, and 6.33 eV at $\alpha_{ac}(8,9) = 0.7$. The energy obtained for $20b_u$ orbital is 7.82 eV at $\alpha_{ac}(6,7) = 2.0$, 7.80 eV at $\alpha_{ac}(7,8) = 1.6$, 7.81 eV at $\alpha_{ac}(8,9) = 1.4$, and 7.46 eV at $\alpha_{ac}(10,11) = 0.8$. Therefore, the energies of the $19b_u$ and $20b_u$ orbitals are 7.72 and 8.09 eV, respectively. The energy obtained for the $21b_u$ orbital is 8.09 eV at $\alpha_{ac}(5,6) = 2.6$. The energy obtained for the $22b_u$ orbital are 9.16 eV at $\alpha_{ac}(7,8) = 2.6$, 9.22 eV at $\alpha_{ac}(8,9) = 2.4$, 9.03 eV at $\alpha_{ac}(8,9) = 1.8$, 8.91 eV at $\alpha_{ac}(10,11) = 1.2$, and 8.76 eV at $\alpha_{ac}(11,12) = 1.0$. Thus, the energy of the $22b_u$ orbital is 9.01 eV.

We then examine the bonding characteristics of unfilled orbitals for $n\text{-}C_4F_{10}$. On the basis of our analysis of the $19a_g$ – $22a_g$, $12a_u$ – $13a_u$, $12b_g$ – $13b_g$, and $18b_u$ – $22b_u$ SKT orbitals, the $19a_g$ orbital is mainly from π_{CC} and σ^*_{CF} . The $20a_g$ orbital is mainly from σ^*_{CF} . The $21a_g$ orbital is mainly from π^*_{CC} and σ^*_{CF} . The $22a_g$ orbital is mainly from π^*_{CC} and σ^*_{CC} . The $12a_u$ orbital is essentially from π -bonding interaction between all neighboring C atoms and σ^*_{CF} . The $13a_u$ orbital is mainly from π_{CC} , π^*_{CC} , and σ^*_{CF} . The $12b_g$ orbital is mainly from π_{CC} , π^*_{CC}

and σ^*_{CF} . The $13b_g$ orbital is essentially from the π -antibonding interaction between each pair of neighboring C atoms. The LUMO $18b_u$ is essentially from the π -bonding interaction between all neighboring C atoms. The $19b_u$ orbital mainly from σ^*_{CF} and π^*_{CF} . The $20b_u$ orbital is mainly from two $-C_2F_5$ groups. The $21b_u$ orbital is mainly from σ^*_{CC} and σ^*_{CF} . The $22b_u$ is essentially from the π -antibonding interaction between each pair of neighboring C atoms and σ^*_{CF} .

For the $n\text{-}C_5F_{12}$ molecule, it has 23 a_1 , 12 a_2 , 15 b_1 , and 19 b_2 occupied orbitals in the C_{2v} point group. The stabilization graphs for the unfilled orbitals of $n\text{-}C_5F_{12}$ have been analyzed in a similar fashion as those of C_2F_6 , C_3F_8 , and $n\text{-}C_4F_{10}$. For the a_1 virtual orbitals, the obtained energies of the $24a_1$ – $29a_1$ orbitals are 1.78, 5.93, 7.39, 7.89, 8.30, and 8.82 eV, respectively. For the a_2 virtual orbitals, the obtained energy of the $13a_2$ and $14a_2$ orbital is 3.81 and 8.11 eV, respectively. For the b_1 virtual orbitals, the obtained energies of the $16b_1$, $17b_1$, and $18b_1$ orbitals are 2.78, 5.77, and 10.31 eV, respectively. For the b_2 virtual orbitals, the energies of the $20b_2$, $21b_2$, $22b_2$, $23b_2$, and $24b_2$ orbitals are 4.98, 6.63, 7.65, 8.35, and 8.84, respectively. According to our analysis of the SKT orbitals for the bonding characteristics of unfilled orbitals of $n\text{-}C_5F_{12}$, the LUMO $24a_1$ orbital is essentially from the π -bonding interaction between all neighboring C atoms. The $25a_1$ orbital is mainly from σ^*_{CF} and π^*_{CF} . Orbitals $26a_1$ and $27a_1$ are mainly from σ^*_{CC} and σ^*_{CF} . Orbital $28a_1$ is essentially from σ^*_{CF} . The $29a_1$ orbital is essentially from antibonding interaction between each pair of neighboring C atoms. The $13a_2$ and $14a_2$ orbitals are mainly from π and π^* interactions between each pair of neighboring C atoms in two $-C_2F_5$ groups, respectively. The $16b_1$ orbital is essentially from the π -bonding interaction between all neighboring C atoms. The $17b_1$ orbital is mainly from π_{CC} , π^*_{CC} , and σ^*_{CF} . The $18b_1$ orbital is essentially from the π -antibonding interaction between each pair of neighboring C atoms. The $20b_2$ orbital is mainly from π_{CC} and σ^*_{CF} of two $-C_2F_5$ groups. MO $21b_2$ is mainly from π^*_{CF} . MO $22b_2$ is essentially from σ^*_{CF} of two $-CF_3$ groups. The $23b_2$ orbital is mainly from σ^*_{CC} of two $-C_2F_5$ groups. The $24b_2$ orbital is essentially from π^*_{CC} and σ^*_{CF} .

Table 3 tabulates the calculated AEs of C_3F_8 , $n\text{-}C_4F_{10}$, and $n\text{-}C_5F_{12}$ via the SKT LC- ω PBE, LC-TPSSTPSS, and LC-BLYP methods using basis set A1 along with the experimental values. For C_3F_8 , our calculations yield two unfilled orbitals ($17a_1$ and $11b_1$) with energies around 3 eV, two orbitals ($13b_2$ and $8a_2$) with energies around 6 eV, and six orbitals ($18a_1$, $14b_2$, $19a_1$, $20a_1$, $15b_2$, and $12b_1$) with energies in the 7–10 eV region. Previous studies by Ishii et al.⁴ have identified the resonances at 3.34 and 6.00 eV. In addition, Tossell et al.⁷ have identified the resonances at 3.6 and 6.1 eV along with the broad peak near 9 eV. Our calculations are in agreement with their experimental results. For $n\text{-}C_4F_{10}$, our calculations yield three unfilled orbitals ($18b_u$, $12a_u$, and $12b_g$) with energies below ~5 eV and ten orbitals ($19a_g$, $19b_u$, $13a_u$, $20b_u$, $20a_g$, $21b_u$, $21a_g$, $22a_g$, $22b_u$, and $13b_g$) with energies in the 6–10 eV region. As for $n\text{-}C_5F_{12}$, three orbitals ($24a_1$, $16b_1$, and $13a_2$) are with energies below 4 eV, three orbitals ($20b_2$, $17b_1$, and $25a_1$) are with energies between 5 and 6 eV, and ten orbitals ($21b_2$, $26a_1$, $22b_2$, $27a_1$, $14a_2$, $28a_1$, $23b_2$, $29a_1$, $24b_2$, and $18b_1$) are with energies in the 7–10 eV region. Previous studies by Ishii et al.⁴ reported the resonance features at 2.37 and 4.63 eV for $n\text{-}C_4F_{10}$ and at 1.64, 3.82, and 5.40 eV for $n\text{-}C_5F_{12}$, respectively.

According to our stabilization calculations for the assignments of the shape resonance observed in ET spectrum⁴ on

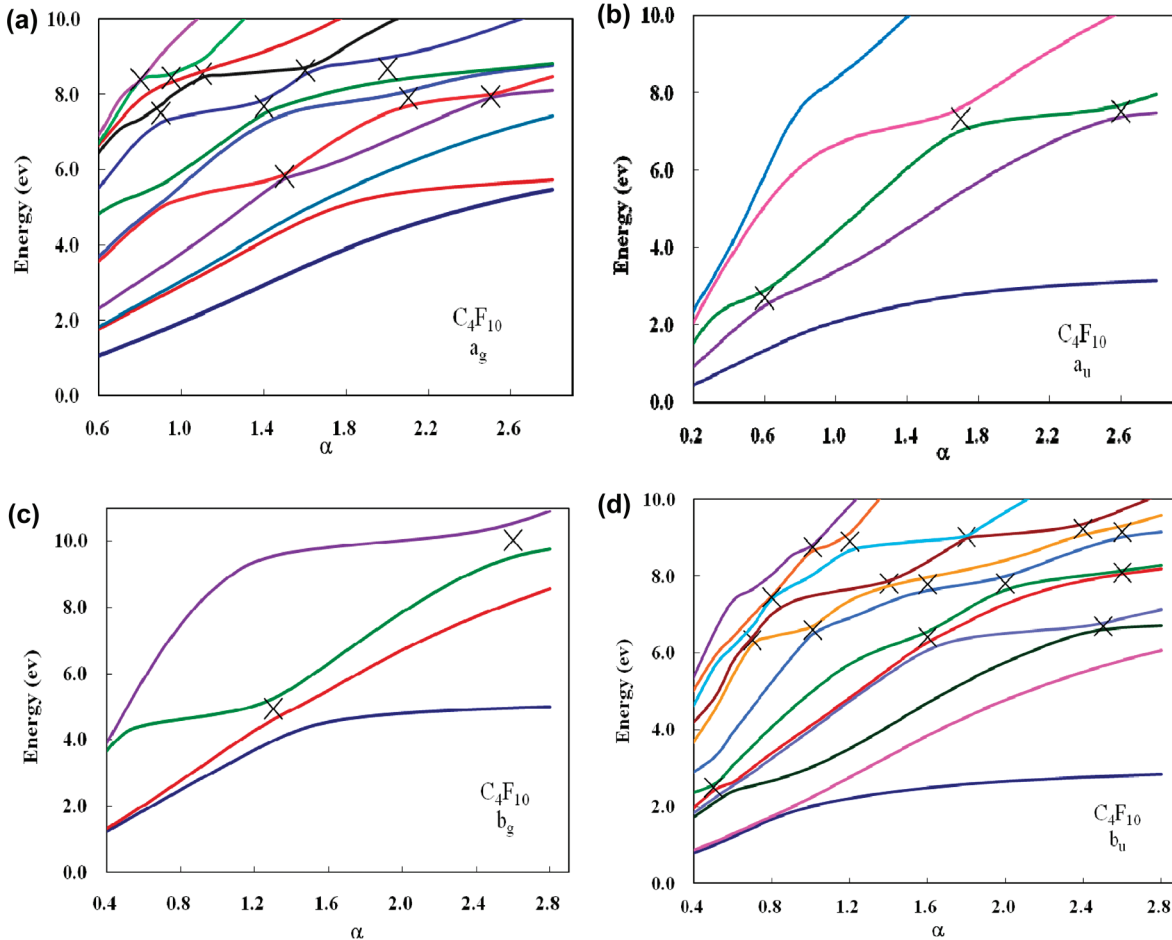


Figure 7. Stabilization graphs for $n\text{-C}_4\text{F}_{10}$ via SKT^{LC- ω PBE} method using basis set A1. Energies of (a) a_g , (b) a_u , (c) b_g , and (d) b_u virtual orbitals as a function of α . The locations of α_{ac} are marked with \times .

C_3F_8 , the electron capture into $17a_1$ and $11b_1$ orbitals corresponds to the resonance at 3.34 eV. The 6.00 eV feature can be ascribed to the electron capture into $8a_2$ and $13b_2$ orbitals. For $n\text{-C}_4\text{F}_{10}$, the electron capture into $18b_u$ and $12a_u$ orbitals corresponds to the resonance at 2.37 eV. The 4.63 eV feature is ascribed to the electron capture into the $12b_g$ orbital. As for $n\text{-C}_5\text{F}_{12}$, the electron capture into the $24a_1$ orbital corresponds to the resonance at 1.64 eV. The 3.82 eV feature is ascribed to the electron capture into $16b_1$ and $13a_2$ orbitals. The 5.40 eV feature is ascribed to the electron capture into $20b_2$, $17b_1$, and $25a_1$ orbitals.

Finally, for $c\text{-C}_3\text{F}_6$ and $c\text{-C}_4\text{F}_8$, the SKT calculations are performed for the representative LC- ω PBE method using basis set A1. The $c\text{-C}_3\text{F}_6$ molecule has six a'_1 , one a'_2 , one a''_1 , four a''_2 , seven-pair e' , and five-pair e'' occupied orbitals in the D_{3h} point group. The stabilization graphs of $c\text{-C}_3\text{F}_6$ for the a'_1 , a'_2 , a''_2 , e' , and e'' virtual orbitals via the SKT^{LC- ω PBE} method using basis set A1 are shown in Figure 8a–e. Nine unfilled orbitals ($7a'_1$, $2a'_2$, $5a''_2$, $8e'$, $9e'$, and $6e''$) are found below ~ 10 eV. For the a'_1 virtual orbitals as shown in Figure 8a, the energy obtained for the $7a'_1$ orbital is 6.81 eV at $\alpha_{ac}(2,3) = 1.6$. For the a'_2 virtual orbitals as shown in Figure 8b, the energies of the $2a'_2$ obtained from the avoided crossings are 5.74 eV at $\alpha_{ac}(1,2) = 1.3$ and 5.70 eV at $\alpha_{ac}(2,3) = 0.4$. Thus, the obtained energy of the $2a'_2$ orbital is 5.72 eV. For the a''_2 virtual orbitals as shown in Figure 8c, the energy obtained for the $5a''_2$ orbital is 1.49 eV at $\alpha_{ac}(1,2) = 0.5$. For the e' virtual orbitals as shown in Figure 8d, the

energies of the $8e'$ obtained from the avoided crossing are 6.88 eV at $\alpha_{ac}(2,3) = 2.0$, 6.96 eV at $\alpha_{ac}(3,4) = 1.2$, and 6.27 eV at $\alpha_{ac}(4,5) = 0.6$. The energies of the $9e'$ obtained from the avoided crossing are 10.21 eV at $\alpha_{ac}(4,5) = 1.8$, 9.99 eV at $\alpha_{ac}(5,6) = 1.1$, and 10.01 eV at $\alpha_{ac}(6,7) = 0.9$. Thus, the obtained energies of the $8e'$ and $9e'$ orbitals are 6.70 and 10.0 eV, respectively. For the e'' virtual orbitals as shown in Figure 8e, the energies of the $6e''$ obtained from the avoided crossings are 10.12 eV at $\alpha_{ac}(1,2) = 2.8$ and 9.92 eV at $\alpha_{ac}(2,3) = 1.2$. Therefore, the energy of the $6e''$ orbital is 10.02 eV. Notice that in the stabilization plots of Figures 5a,d, 7a,d, and 8e where the avoided crossing pattern is very complex, we have performed DOS analysis and have confirmed that the obtained orbital energies are very close to our obtained results (the differences in energy are < 0.1 eV). As illustrated in the stabilization plots, some cases (such as Figures 5b,c and 8a,c,e) have only exhibited one or two avoided crossings. To ensure that the basis set is sufficiently flexible to provide reliable estimates for the resonance energies in these cases, we have performed additional calculations with A5 and B2 basis sets for the resonance energies via the SKT^{LC- ω PBE} method for comparison. When these more diffuse base sets are used, the changes in resonance energy are within 0.2 eV. Hence, the present A1 basis set can provide reliable estimates for the resonance energies. Figure 9 displays the $5a''_2$, $2a'_2$, $7a'_1$, $8e'$, $9e'$, and $6e''$ SKT orbitals for $\alpha = 1.0$ of $c\text{-C}_3\text{F}_6$. They are the first a''_2 , second a'_2 , third a'_1 , fourth e' , sixth e' , and third e'' virtual orbitals of $\alpha =$

Table 3. Calculated AEs (eV) of C_3F_8 , $n\text{-}C_4F_{10}$, and $n\text{-}C_5F_{12}$ Using Basis Set A1

method		SKT ^{LC-ωPBE}	SKT ^{LC-TPSSTPSS}	SKT ^{LC-BLYP}	exptl ^a	exptl ^b
C_3F_8	17a ₁	3.39	3.43	3.38	3.34	3.6
	11b ₁	3.46	3.64	3.48	6.00	6.1
	13b ₂	6.01	6.22	6.10		9.0
	8a ₂	6.28	6.42	6.19		
	18a ₁	7.55	7.62	7.21		
	14b ₂	7.79	8.09	7.66		
	19a ₁	7.90	8.29	7.80		
	20a ₁	8.72	8.86	8.68		
	15b ₂	8.98	9.12	9.07		
	12b ₁	9.54	9.67	9.40		
$n\text{-}C_4F_{10}$	18b _u	2.49	2.49	2.48	2.37	
	12a _u	2.69	2.73	2.71	4.63	
	12b _g	4.93	5.02	4.98		
	19a _g	5.82	5.91	5.81		
	19b _u	6.58	6.72	6.39		
	13a _u	7.42	7.51	7.04		
	20b _u	7.72	7.92	7.64		
	20a _g	7.76	7.95	7.44		
	21b _u	8.09	8.22	8.03		
	21a _g	8.43	8.55	8.34		
$n\text{-}C_5F_{12}$	22a _g	8.63	8.82	8.58		
	22b _u	9.01	9.06	8.62		
	13b _g	10.02	10.17	9.68		
	24a ₁	1.78	1.76	1.77	1.64	
	16b ₁	2.78	2.82	2.79	3.82	
	13a ₂	3.81	3.88	3.86	5.40	
	20b ₂	4.98	5.06	4.95		
	17b ₁	5.77	5.88	5.82		
	25a ₁	5.93	6.05	5.82		
	21b ₂	6.63	6.77	6.63		
	26a ₁	7.39	7.59	7.29		
	22b ₂	7.65	7.76	7.39		
	27a ₁	7.89	8.01	7.85		
	14a ₂	8.11	8.25	8.07		
	28a ₁	8.30	8.46	8.15		
	23b ₂	8.35	8.52	8.13		
	29a ₁	8.82	8.93	8.56		
	24b ₂	8.84	8.99	8.80		
	18b ₁	10.31	10.31	10.15		

^aReference 4. ^bReference 7.

1.0. As can be seen in Figure 9, the LUMO ($5a_2''$) is essentially from the π -bonding interaction between all neighboring C atoms and σ_{CF}^* . The $2a_2'$ orbital is essentially from σ_{CC}^* and π_{CF}^* . The $7a_1'$ orbital corresponds to bonding interaction between all C atoms and σ_{CF}^* . The $8e'$ orbitals are mainly from σ_{CF}^* and σ_{CC}^* . The $9e'$ orbitals are mainly from σ_{CC}^* , π_{CC}^* , and σ_{CF}^* . The $6e''$ orbitals are essentially from π_{CC}^* , π_{CC}^* , and σ_{CF}^* .

The stabilization graphs for the unfilled orbitals of $c\text{-}C_4F_8$ have been analyzed in a similar fashion as those of other PFAs. For the a_1 virtual orbitals, the obtained energies of the $11a_1$ – $12a_1$ orbitals are 7.12 and 11.25 eV, respectively. For the a_2 virtual orbitals, the obtained energy of the $3a_2$ orbital is 7.82 eV. For the b_2 virtual orbitals, the obtained energies of the $10b_2$ – $12b_2$ orbitals are 0.82, 7.63, and 12.39 eV, respectively. For the e virtual orbitals, the energies of the $13e$ – $15e$ orbitals are 5.45, 7.27, and 8.50, respectively. According to our analysis of the SKT orbitals for the bonding characteristics of unfilled orbitals of $c\text{-}C_4F_8$ in D_{2d} , the $11a_1$ orbital is essentially from the bonding interaction between all C atoms and σ_{CF}^* . The $12a_1$ orbital is

mainly from π -antibonding interaction between all neighboring C atoms mixing with σ_{CF}^* . The $3a_2$ orbital is essentially from σ_{CC}^* and π_{CF}^* . The LUMO $10b_2$ corresponds to π -bonding interaction between all neighboring C atoms and σ_{CF}^* . The $11b_2$ orbital is essentially from σ_{CC}^* and σ_{CF}^* . The $12b_2$ orbital is mainly from antibonding interaction between all neighboring C atoms and π_{CF}^* . The $13e$ orbitals are essentially from π_{CF}^* . The $14e$ and $15e$ orbitals are essentially from σ_{CF}^* .

Table 4 tabulates the calculated AEs of $c\text{-}C_3F_6$ and $c\text{-}C_4F_8$ for the SKT^{LC- ω PBE} method using basis set A1 along with the experimental values. According to Table 4 for $c\text{-}C_3F_6$, our calculations yield one unfilled orbital ($5a_2''$) with energy around 1.5 eV, one orbital ($2a_2'$) with energies around 5.7 eV, two orbitals ($7a_1'$ and $8e'$) with energies around 7 eV, and two orbitals ($9e'$ and $6e''$) with energies around 10 eV. As can be seen from the results, our calculations are in agreement with those of the previous studies by Ishii et al.⁴ They identified the resonances at 1.27, 5.74, and 7.26 eV. As for $c\text{-}C_4F_8$, our calculations yield one unfilled orbital ($10b_2$) with energy

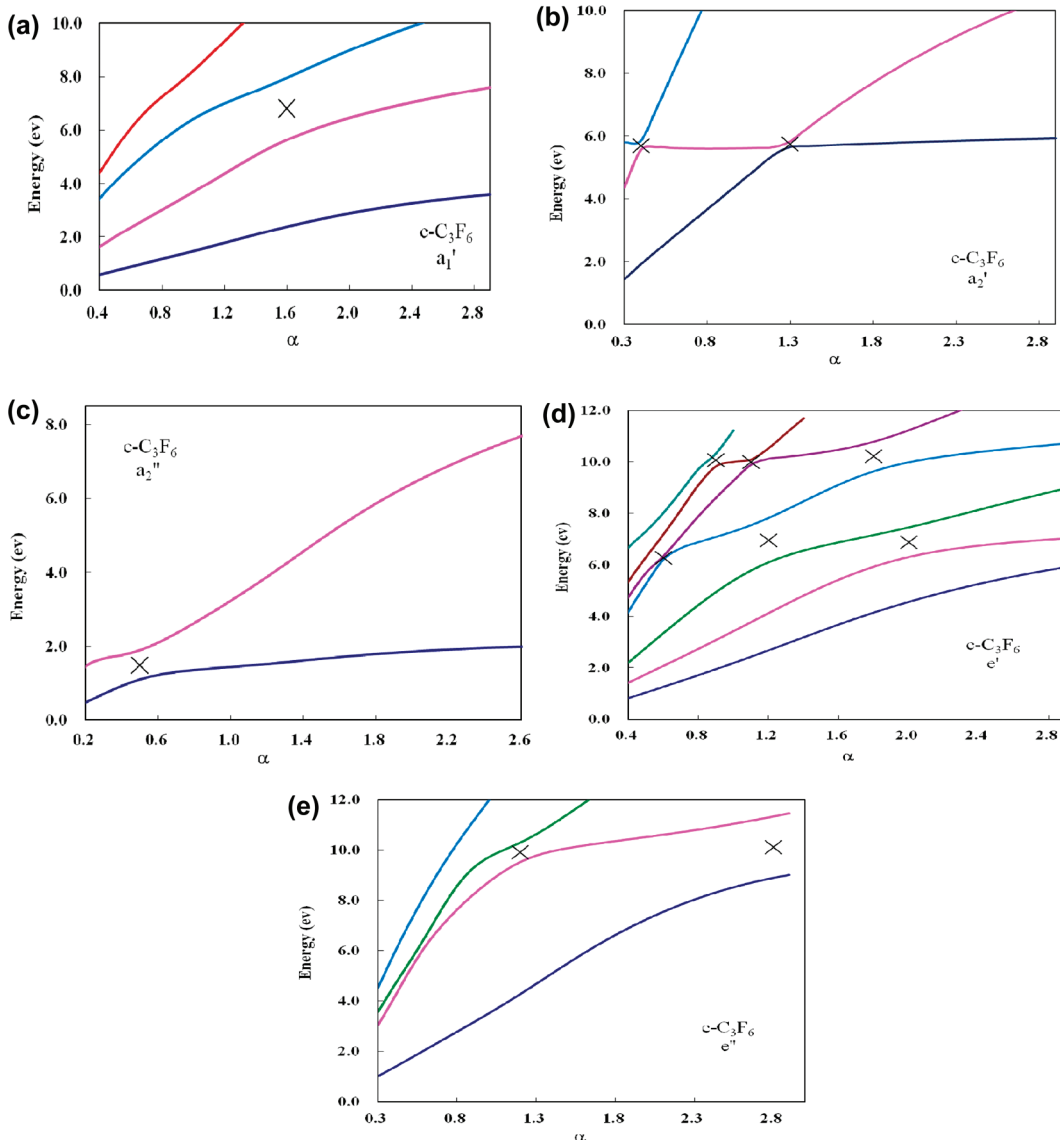


Figure 8. Stabilization graphs for $c\text{-C}_3\text{F}_6$ via the SKT^{LC- ω PBE} method using basis set A1. Energies of (a) a_1' , (b) a_2' , (c) a_2'' , (d) e' , and (e) e'' virtual orbitals as a function of α . The locations of α_{ac} are marked with X.

around 1 eV, one orbital ($13e$) with energy around 5 eV, five orbitals ($11a_1$, $14e$, $11b_2$, $3a_2$, and $15e$) with energies in the 7–9 eV region, and two orbitals ($11a_1$ and $12b_2$) with energies around 12 eV. Previous scattering calculations by Winstead and McKoy⁹ have also identified three $^2\text{B}_2$, two ^2E , two $^2\text{A}_1$, and one $^2\text{A}_2$ resonance states for $c\text{-C}_4\text{F}_8$, but their resonance energies are larger (~ 3 eV) than ours. Previous ET spectrum studies by Ishii et al.⁴ reported the resonances at 4.91 eV. Christophorou and Olthoff⁶ suggested the resonances were at -0.6, 4.9, 6.9, 9.0, and 10.5 eV, which were close to our calculated positions except for the first $^2\text{B}_2$ anion state. According to our stabilization calculations for the assignments of the shape resonance observed in ET spectrum⁴ on $c\text{-C}_3\text{F}_6$, the electron capture into the $5a_2''$ orbital corresponds to the resonance at 1.27 eV. The 5.74 eV feature can be ascribed to the electron capture into the $2a_2'$ orbital. The 7.25 eV feature can be ascribed to the electron capture into $8e'$ and $7a'$ orbitals. For $c\text{-C}_4\text{F}_8$, the electron capture into $13e$ orbitals corresponds to the resonance at 4.91 eV. The electron addition to other orbitals may not be observed in the ET spectrum. Finally, by comparing

Tables 1, 3, and 4, our results have indicated that the lowest resonance energies decrease as the sizes of the perfluoroalkanes increase. In addition, the lowest resonance energies of the $c\text{-C}_3\text{F}_6/c\text{-C}_4\text{F}_8$ are lower than those of the corresponding $n\text{-C}_3\text{F}_8/n\text{-C}_4\text{F}_{10}$.

4. CONCLUSIONS

The energies of unfilled orbitals in $n\text{-C}_n\text{F}_{2n+2}$ ($n = 2\text{--}5$), $c\text{-C}_3\text{F}_6$, and $c\text{-C}_4\text{F}_8$ have been systematically studied via various LRC-DFT methods. Results have demonstrated that the SKT method can yield much better energy results of temporary anion states than the KT method without stabilization. The key factor for the superiority of the SKT approach is the adoption of the stabilization method that enables us to distinguish the temporary anion state solutions from ODC solutions in virtual orbitals. As a result, the presence of several more temporary anion states for n -PFAs and c -PFAs has been identified. It is believed that this SKT approach can be very useful in studying the temporary anion states of PFAs.

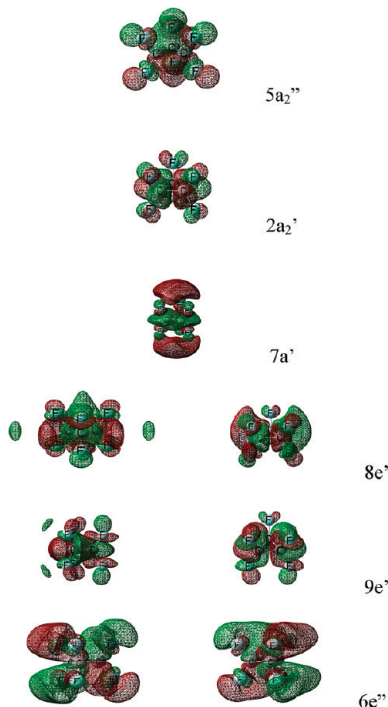


Figure 9. Plots of the $5a_2''$, $2a_2'$, $7a_1'$, $8e'$, $9e'$, and $6e''$ SKT orbitals at $\alpha = 1.0$ for $c\text{-C}_3\text{F}_6$. The isosurface values are chosen to be 0.02 for all the MO plots.

Table 4. Calculated AEs (eV) of $c\text{-C}_3\text{F}_6$ and $c\text{-C}_4\text{F}_8$ Using the SKT^{LC- ω PBE} Method

method	SKT ^{LC-ωPBE}	theory ^a	exptl ^b	exptl ^c
$c\text{-C}_3\text{F}_6$	$5a_2''$	1.49		1.27
	$2a_2'$	5.72		5.74
	$8e'$	6.70		7.25
	$7a_1'$	6.81		
	$9e'$	10.00		
	$6e''$	10.02		
$c\text{-C}_4\text{F}_8$	$10b_2$	0.82	3.0	4.91
	$13e$	5.45	8.1	4.9
	$11a_1$	7.12	6.8	6.9
	$14e$	7.27	10.0	9.0
	$11b_2$	7.63	12.5	10.5
	$3a_2$	7.82	10.6	
	$15e$	8.50	14.7	
	$12a_1$	12.25	16.0	
	$12b_2$	12.39	16.4	

^aReference 9. ^bReference 4. ^cReference 6.

AUTHOR INFORMATION

Corresponding Author

*Tel: 011-886-4-23590248-102. Fax: 011-886-4-23590426. E-mail: hycheng@thu.edu.tw.

Notes

The authors declare no competing financial interest.

ACKNOWLEDGMENTS

We would like to thank the reviewers for valuable comments during the revision process and National Center for High-Performance Computing for the computational resources provided. This work was supported by the National Science

Council of Republic of China under grant number NSC 100-2113-M029-004.

REFERENCES

- (a) Slinn, D. S. L.; Green, S. W. In *Preparation, Properties and Industrial Applications of Organofluorine Compounds*; Banks, R. E., Ed.; Ellis Harwood: Chichester, U.K., 1982; p 45. (b) Banks, R. E.; Sharp, D. W. A.; Tatlow, J. C., Eds. *Fluorine: The First 100 Years*; Elsevier: New York, 1986. (c) Green, S. W.; Slinn, D. S. L.; Simpson, R. N. F.; Woytek, A. J. In *Organofluorine Chemistry, Principles and Commercial Applications*; Banks, R. E., Smart, B. E., Tatlow, J. C., Eds.; Plenum: New York, 1994; p 89. (d) Kajdas, C. Industrial Lubricants. In *Chemistry and Technology of Lubricants*; Mortier, R. M., Orszulik, S. T., Eds.; VCH Publishers: New York, 1992. (e) Ogino, K.; Abe, M. *Mixed Surfactant Systems*; M. Dekker, Inc.: New York, 1993. (f) Horvath, I. T.; Rabai, J. *Science* **1994**, *266*, 72. (g) Horvath, I. T. *Acc. Chem. Res.* **1998**, *31*, 641. (h) Sandford, G. *Tetrahedron* **2003**, *59*, 437. (i) Hatano, Y. *Adv. At. Mol. Opt. Phys.* **2002**, *43*, 231. (j) Eastoe, J.; Bayazit, Z.; Martel, S.; Steytler, D. C.; Heenan, R. K. *Langmuir* **1996**, *12*, 1423. (k) Riess, J. G. *Chem. Rev.* **2001**, *101*, 2797.
- (2) Sanche, L.; Schulz, G. *J. Phys. Rev. A* **1972**, *5*, 1672.
- (3) Jordan, K. D.; Burrow, P. D. *Chem. Rev.* **1987**, *87*, 557.
- (4) Ishii, I.; McLaren, R.; Hitchcock, A. P.; Jordan, K. D.; Choi, Y.; Robin, M. B. *Can. J. Chem.* **1988**, *66*, 2104.
- (5) (a) Spyrou, S. M.; Sauers, I.; Christopoulou, L. G. *J. Chem. Phys.* **1983**, *78*, 7200. (b) Hunter, S. R.; Christopoulou, L. G. *J. Chem. Phys.* **1984**, *80*, 6150. (c) Spyrou, S. M.; Christopoulou, L. G. *J. Chem. Phys.* **1985**, *82*, 2620. (d) Spyrou, S. M.; Christopoulou, L. G. *J. Chem. Phys.* **1985**, *83*, 2829. (e) Spyrou, S. M.; Hunter, S. R.; Christopoulou, L. G. *J. Chem. Phys.* **1985**, *83*, 641. (f) Hunter, S. R.; Carter, J. G.; Christopoulou, L. G. *J. Chem. Phys.* **1987**, *86*, 693. (g) Hunter, S.; Carter, J.; Christopoulou, L. G. *Phys. Rev. A* **1988**, *38*, 58. (h) Christopoulou, L. G.; Olthoff, J. K.; Rao, M. V. V. S. *J. Phys. Chem. Ref. Data* **1996**, *25*, 1341. (i) Christopoulou, L. G.; Olthoff, J. K. *J. Phys. Chem. Ref. Data* **1999**, *28*, 967.
- (6) Christopoulou, L. G.; Olthoff, J. K. *J. Phys. Chem. Ref. Data* **2001**, *30*, 449.
- (7) Sanabria, J. E.; Cooper, G. D.; Tossell, J. A.; Moore, J. H. *J. Chem. Phys.* **1998**, *108*, 389.
- (8) (a) Takagi, T.; Boesten, L.; Tanaka, H.; Dillon, M. A. *J. Phys. B* **1994**, *27*, 5389. (b) Weik, F.; Illenberger, E. *J. Chem. Phys.* **1995**, *99*, 1406. (c) Jelisavcic, M.; Panajotovic, R.; Kitajima, M.; Hoshino, M.; Tanaka, H.; Buckman, S. J. *J. Chem. Phys.* **2004**, *121*, 5272.
- (9) Winstead, C.; McKoy, V. *J. Chem. Phys.* **2001**, *114*, 7407.
- (10) (a) Paul, A.; Wannere, C.; Schaefer, H. F. *III. J. Phys. Chem. A* **2004**, *108*, 9428. (b) Paul, A.; Wannere, C.; Kasalova, V.; Schleyer, P. R.; Schaefer, H. F. *III. J. Am. Chem. Soc.* **2005**, *127*, 15457. (c) Paul, A.; Schleyer, P. V. R.; Schaefer, H. F. *III. Mol. Phys.* **2006**, *104*, 1311.
- (11) (a) Simons, J. *J. Phys. Chem. A* **2008**, *112*, 6401. (b) Simons, J. *Annu. Rev. Phys. Chem.* **2011**, *62*, 107. (c) Sommerfeld, T.; Weber, R. J. *J. Phys. Chem. A* **2011**, *115*, 6675.
- (12) Koopmans, T. *Physica* **1934**, *1*, 104.
- (13) Falsetta, M. F.; Jordan, K. D. *J. Phys. Chem.* **1990**, *94*, 5666.
- (14) (a) Falsetta, M. F.; Jordan, K. D. *J. Am. Chem. Soc.* **1991**, *113*, 2903. (b) Falsetta, M. F.; Jordan, K. D. *Chem. Phys. Lett.* **1999**, *300*, 588.
- (15) Falsetta, M. F.; Choi, Y.; Jordan, K. D. *J. Phys. Chem. A* **2000**, *104*, 9605.
- (16) Burrow, P. D.; Howard, A. E.; Johnston, A. R.; Jordan, K. D. *J. Phys. Chem.* **1992**, *96*, 7570.
- (17) (a) Juang, C.-Y.; Chao, J. S.-Y. *J. Phys. Chem.* **1994**, *98*, 13506. (b) Chen, C.-S.; Feng, T.-H.; Chao, J. S.-Y. *J. Phys. Chem.* **1995**, *99*, 8629. (c) Wei, Y.-H.; Cheng, H.-Y. *J. Phys. Chem. A* **1998**, *102*, 3560.
- (18) (a) Hazi, A. U.; Taylor, H. S. *Phys. Rev. A* **1970**, *1*, 1109. (b) Taylor, H. S. *Adv. Chem. Phys.* **1970**, *18*, 91. (c) Fels, M. F.; Hazi, A. U. *Phys. Rev. A* **1972**, *5*, 1236. (d) Taylor, H. S.; Hazi, A. U. *Phys. Rev. A* **1976**, *14*, 2071.
- (19) (a) Chao, J. S.-Y. *Chem. Phys. Lett.* **1991**, *179*, 169. (b) Chao, J. S.-Y. *J. Phys. Chem.* **1993**, *97*, 4016.

- (20) Kohn, W.; Sham, L. J. *Phys. Rev. A* **1965**, *10*, 1133.
- (21) Rienstra-Kiracofe, J. C.; Tschumper, G. S.; Schaefer, H. F. III; Nandi, S.; Ellison, G. B. *Chem. Rev.* **2002**, *102*, 231.
- (22) Vydrov, O. A.; Scuseria, G. E. *J. Chem. Phys.* **2006**, *125*, 234109.
- (23) Chai, J.-D.; Head-Gordon, M. *Phys. Chem. Chem. Phys.* **2008**, *10*, 6615.
- (24) Yanai, T.; Tew, D. P.; Handy, N. C. *Chem. Phys. Lett.* **2004**, *393*, 51.
- (25) (a) Iikura, H.; Tsuneda, T.; Yanai, T.; Hirao, K. *J. Chem. Phys.* **2001**, *115*, 3540. (b) Tsuneda, T.; Song, J.-W.; Suzuki, S.; Hirao, K. *J. Chem. Phys.* **2010**, *113*, 174101.
- (26) (a) Tozer, D. J.; De Proft, F. *J. Phys. Chem. A* **2005**, *109*, 8923. (b) Tozer, D. J.; De Proft, F. *J. Chem. Phys.* **2007**, *127*, 034108. (c) De Proft, F.; Sablon, N.; Tozer, D. J.; Geerlings, P. *Faraday Discuss.* **2007**, *135*, 151. (d) Sablon, N.; De Proft, F.; Geerlings, P.; Tozer, D. *J. Phys. Chem. Chem. Phys.* **2007**, *9*, 5880. (e) Teale, A. M.; De Proft, F.; Tozer, D. *J. J. Chem. Phys.* **2008**, *129*, 044110. (f) Hajgató, B.; Deleuze, M. S.; Tozer, D. J.; De Proft, F. *J. Chem. Phys.* **2008**, *129*, 084308.
- (27) (a) Cheng, H.-Y.; Shih, C.-C. *J. Phys. Chem. A* **2009**, *113*, 1548. (b) Cheng, H.-Y.; Shih, C.-C.; Chang, J.-T. *J. Phys. Chem. A* **2009**, *113*, 9551. (c) Cheng, H.-Y.; Chang, J.-T.; Shih, C.-C. *J. Phys. Chem. A* **2010**, *113*, 2920. (d) Cheng, H.-Y.; Chen, C.-W.; Chang, J.-T.; Shih, C.-C. *J. Phys. Chem. A* **2011**, *115*, 84. (e) Cheng, H.-Y.; Chen, C.-W. *J. Phys. Chem. A* **2011**, *115*, 10113.
- (28) (a) Dunning, T. H. Jr. *J. Chem. Phys.* **1989**, *90*, 1007. (b) Kendall, R. A.; Dunning, T. H. Jr.; Harrison, R. J. *J. Chem. Phys.* **1992**, *96*, 6769.
- (29) (a) The midpoint method is applicable when comparing its results with those obtained from the more rigorous analytic continuation method (ref 19 in ref 17a). (b) The resonance energies can also be obtained by means of density-of-state method. Mandelshtam, V. A.; Ravuri, T. R.; Taylor, H. S. *Phys. Rev. Lett.* **1993**, *70*, 1932. Simons's formula. Simons, J. *J. Chem. Phys.* **1981**, *75*, 2465. Löwdin's scheme. Löwdin, P.-O. *Int. J. Quantum Chem.* **1985**, *27*, 495.
- (30) Perdew, J. P.; Burke, K.; Ernzerhof, M. *Phys. Rev. Lett.* **1996**, *77*, 3865.
- (31) Tao, J. M.; Perdew, J. P.; Staroverov, V. N.; Scuseria, G. E. *Phys. Rev. Lett.* **2003**, *91*, 146401.
- (32) Zhao, Y.; Truhlar, D. G. *J. Chem. Phys.* **2006**, *125*, 194101.
- (33) (a) Grimme, S. *J. Chem. Phys.* **2006**, *124*, 034108. (b) Schwabe, T.; Grimme, S. *Phys. Chem. Chem. Phys.* **2006**, *8*, 4398. (c) Schwabe, T.; Grimme, S. *Phys. Chem. Chem. Phys.* **2007**, *9*, 3397.
- (34) Frisch, M. J.; Trucks, G. W.; Schlegel, H. B.; Scuseria, G. E.; Robb, M. A.; Cheeseman, J. R.; Scalmani, G.; Barone, V.; Mennucci, B.; Petersson, G. A.; Nakatsuji, H.; Caricato, M.; Li, X.; Hratchian, H. P.; Izmaylov, A. F.; Bloino, J.; Zheng, G.; Sonnenberg, J. L.; Hada, M.; Ehara, M.; Toyota, K.; Fukuda, R.; Hasegawa, J.; Ishida, M.; Nakajima, T.; Honda, Y.; Kitao, O.; Nakai, H.; Vreven, T.; Montgomery, J. A., Jr.; Peralta, J. E.; Ogliaro, F.; Bearpark, M.; Heyd, J. J.; Brothers, E.; Kudin, K. N.; Staroverov, V. N.; Kobayashi, R.; Normand, J.; Raghavachari, K.; Rendell, A.; Burant, J. C.; Iyengar, S. S.; Tomasi, J.; Cossi, M.; Rega, N.; Millam, J. M.; Klene, M.; Knox, J. E.; Cross, J. B.; Bakken, V.; Adamo, C.; Jaramillo, J.; Gomperts, R.; Stratmann, R. E.; Yazyev, O.; Austin, A. J.; Cammi, R.; Pomelli, C.; Ochterski, J. W.; Martin, R. L.; Morokuma, K.; Zakrzewski, V. G.; Voth, G. A.; Salvador, P.; Dannenberg, J. J.; Dapprich, S.; Daniels, A. D.; Farkas, O.; Foresman, J. B.; Ortiz, J. V.; Cioslowski, J.; Fox, D. J. *Gaussian 09*, revision A.02; Gaussian, Inc.: Wallingford, CT, 2009.
- (35) (a) Vydrov, O. A.; Scuseria, G. E. *J. Chem. Phys.* **2005**, *122*, 184107. (b) Dutoi, A. D.; Head-Cordon, M. *Chem. Phys. Lett.* **2006**, *422*, 230.